

A concerted systems biology analysis of phenol metabolism in *Rhodococcus opacus* PD630

Garrett W. Roell^a, Rhiannon R. Carr^a, Tayte Campbell^b, Zeyu Shang^a, William R. Henson^a, Jeffrey J. Czajka^a, Hector García Martín^{c,d,e,f}, Fuzhong Zhang^a, Marcus Foston^a, Gautam Dantas^{b,g,h,i}, Tae Seok Moon^{a,**}, Yinjie J. Tang^{a,*}

^a Department of Energy, Environmental and Chemical Engineering, Washington University in St. Louis, St. Louis, MO, 63130, USA

^b The Edison Family Center for Genome Sciences and Systems Biology, Washington University in St. Louis School of Medicine, St. Louis, MO, 63110, USA

^c DOE, Joint BioEnergy Institute, Emeryville, CA, 94608, USA

^d DOE, Agile BioFoundry, Emeryville, CA, 94608, USA

^e Biological Systems and Engineering Division, Lawrence Berkeley National Lab, Berkeley, CA, 94720, USA

^f BCAM, Basque Center for Applied Mathematics, Bilbao, Spain

^g Department of Pathology and Immunology, Washington University in St. Louis School of Medicine, St. Louis, MO, 63108, USA

^h Department of Biomedical Engineering, Washington University in St. Louis, St. Louis, MO, 63130, USA

ⁱ Department of Molecular Microbiology, Washington University in St. Louis School of Medicine, St. Louis, MO, 63108, USA

ARTICLE INFO

Keywords:

¹³C-MFA

¹³C-pulse-tracing

Entner–Doudoroff pathway

Gluconeogenesis

Lignin

ABSTRACT

Rhodococcus opacus PD630 metabolizes aromatic substrates and naturally produces branched-chain lipids, which are advantageous traits for lignin valorization. To provide insights into its lignocellulose hydrolysate utilization, we performed ¹³C-pathway tracing, ¹³C-pulse-tracing, transcriptional profiling, biomass composition analysis, and metabolite profiling in conjunction with ¹³C-metabolic flux analysis (¹³C-MFA) of phenol metabolism. We found that 1) phenol is metabolized mainly through the ortho-cleavage pathway; 2) phenol utilization requires a highly active TCA cycle; 3) NADPH is generated mainly via NADPH-dependent isocitrate dehydrogenase; 4) active cataplerotic fluxes increase plasticity in the TCA cycle; and 5) gluconeogenesis occurs partially through the reversed Entner–Doudoroff pathway (EDP). We also found that phenol-fed *R. opacus* PD630 generally has lower sugar phosphate concentrations (e.g., fructose 1,6-bisphosphatase) compared to metabolite pools in ¹³C-glucose-fed *Escherichia coli* (set as internal standards), while its TCA metabolites (e.g., malate, succinate, and α -ketoglutarate) accumulate intracellularly with measurable succinate secretion. In addition, we found that phenol utilization was inhibited by benzoate, while catabolite repressions by other tested carbon substrates (e.g., glucose and acetate) were absent in *R. opacus* PD630. Three adaptively-evolved strains display very different growth rates when fed with phenol as a sole carbon source, but they maintain a conserved flux network. These findings improve our understanding of *R. opacus*' metabolism for future lignin valorization.

1. Introduction

Engineering bacterial cells to utilize lignocellulosic biomass as a feedstock could offer cost-competitive production of renewable fuels, chemicals, and materials (Ragauskas et al., 2006). Lignocellulosic biomass is composed mainly of cellulose, hemicellulose, and lignin. Lignocellulosic carbohydrates, specifically cellulose and hemicellulose, can

be deconstructed into fermentable sugars for biological conversion into a range of bioproducts. Lignocellulose is a recalcitrant feedstock for biological conversion, in part due to its up to 35% lignin content (Gani and Naruse, 2007). Pretreatments are employed prior to carbohydrate deconstruction to increase sugar monomer content and thus product yield. However, lignin degradation during pretreatment often produces aromatic compounds that strongly inhibit the growth of most bacteria

* Corresponding author.

** Corresponding author.

E-mail addresses: garrettroell@wustl.edu (G.W. Roell), rrcarr@wustl.edu (R.R. Carr), tayte.campbell@gmail.com (T. Campbell), Zeyu.Shang@wustl.edu (Z. Shang), williamrhenson@gmail.com (W.R. Henson), jjczajka@umich.edu (J.J. Czajka), hgmartin@lbl.gov (H.G. Martín), fzhang29@wustl.edu (F. Zhang), mfoston@wustl.edu (M. Foston), dantas@wustl.edu (G. Dantas), tsmoon@wustl.edu (T.S. Moon), yinjie.tang@seas.wustl.edu (Y.J. Tang).

<https://doi.org/10.1016/j.ymben.2019.06.013>

Received 21 January 2019; Received in revised form 19 June 2019; Accepted 30 June 2019

Available online 02 July 2019

1096-7176/ © 2019 International Metabolic Engineering Society. Published by Elsevier Inc. All rights reserved.

(Beckham et al., 2016). Moreover, conventional fermentative biorefineries treat lignin as by-product, and burn it for low-value electricity or process heat (Ragauskas et al., 2014). Techno-economic analyses have reported that the use of lignin for co-product generation is a key to profitable lignocellulose valorization (Valdivia et al., 2016). Lignin cannot be rapidly broken down by biological methods (Boerjan et al., 2003; Studer et al., 2011). Thus, an approach for lignin utilization has been proposed that combines the rapid depolymerization kinetics of chemical processing with the metabolic funneling and selective abilities of microbial systems (Linger et al., 2014; Wheeldon et al., 2017). Recently, research groups have attempted to develop microbial hosts with improved tolerance to aromatic compounds for fermentation of lignocellulose-derived sugars and lignin-derived aromatic compounds (Abdelaziz et al., 2016; Ragauskas et al., 2014; Janusz et al., 2017). In particular, lignin-rich streams have been utilized to generate lipid-based biofuels (i.e., waste-to-fuel applications) (Le et al., 2017; Yaguchi et al., 2017).

Rhodococcus opacus PD630 (hereafter *R. opacus*) is a Gram-positive actinobacterium. It is natively able to utilize sugars, aromatics, furans, and organic acids (Holder et al., 2011; Kurosawa et al., 2015). Isolated from a gas works plant, this strain is capable of accumulating triacylglycerol (TAG), the precursor for biodiesel, up to 80% of its dry cell weight (Alvarez et al., 1996). Studies of its mechanisms of aromatic tolerance and TAG accumulation have found promising results for its use in the conversion of lignin-derived aromatic substrates (DeLorenzo et al., 2017; Henson et al., 2018a, 2018b; Yoneda et al., 2016). *R. opacus* has been extensively studied for its growth kinetics and transcriptional activities, yet key knowledge gaps linking genotype to phenotype still remain. Specifically, there is little knowledge about the distribution of the metabolic fluxes in this biofuel producer when consuming aromatic substrates, including ambiguity over whether the ortho or meta bond of catechol is broken during ring opening. Functional characterization of the central metabolic network is necessary to develop this nonmodel platform for metabolic engineering applications, particularly to facilitate genome-scale modeling for rational strain design.

In this work, we have characterized phenol-fed cultures of *R. opacus* based on integrated omics analyses. ^{13}C -metabolic flux analysis (^{13}C -MFA) can measure *in vivo* reaction rates of central metabolism and confirm global gene regulation patterns inferred from transcriptomic data (Chubukov et al., 2013). In the past, ^{13}C -MFA mostly focused on cellular metabolisms fed with sugars, organic acids, and CO_2 (photosynthesis). To our knowledge, this work is the first report of a full MFA completed in any organism using phenol as the sole carbon source. Additionally, we performed ^{13}C -pathway tracing, metabolite analysis, flux balance analysis, and biomass composition analysis. The flux-based insights were further connected to recently reported transcriptional profiles and proteomics data. We also examined how adaptive laboratory evolution affects the central flux network. These systems analyses provide a deeper understanding of *R. opacus* metabolism of lignin-derived substrates at different layers of cellular processes.

2. Materials and methods

2.1. Chemicals, strains, and growth conditions

$1\text{-}^{13}\text{C}$ phenol, $2,6\text{-}^{13}\text{C}$ phenol, and $\text{U-}^{13}\text{C}$ phenol were purchased from Cambridge Isotope Laboratories Inc. (Tewksbury, MA, USA). All other chemicals were purchased from Sigma-Aldrich (St. Louis, MO, USA). All cells were grown in minimal media, previously described as media B (DeLorenzo et al., 2017). Unless otherwise noted, the sole carbon source was 0.5 g/L phenol, and the nitrogen source was 1 g/L ammonium sulfate. For all cultures, a single colony of *R. opacus* from a tryptic soy broth plate was inoculated into 2 mL minimal medium, which was used as a seed culture for 10 mL cultures. Isotopomer measurements were conducted when cell cultures reached an optical

density at 600 nm (OD_{600}) of 0.2–0.5, corresponding to exponential growth.

2.2. Analysis of proteinogenic amino acid labeling

10 mL labeled biomass from $2,6\text{-}^{13}\text{C}$ phenol or $1\text{-}^{13}\text{C}$ phenol growing cultures (biological duplicates, $n = 2$) were centrifuged down then hydrolyzed at $100\text{ }^\circ\text{C}$ for 24 h. The resulting amino acids were analyzed by GC-MS via the TBDMS (N-(tert-butyltrimethylsilyl)-N-methyltrifluoroacetamide) method as described previously (You et al., 2012). In brief, the $[\text{m-57}]^+$ and $[\text{m-159}]^+$ fragments for amino acids were mainly used for ^{13}C -MFA, while the $[\text{m-15}]^+$, $[\text{m-85}]^+$, and $f(302)^+$ fragments were also analyzed to provide additional labeling information. The $\text{m}+0$, $\text{m}+1$, $\text{m}+2$, etc. data corresponds to the fraction of fragments that were unlabeled, singly labeled, doubly labeled, etc. Labeling data were corrected for naturally-occurring isotopes.

2.3. Dynamic labeling (pulse-tracing), free metabolite extraction, and LC-MS analysis

For phenol dynamic labeling experiments, 20 mL unlabeled phenol cultures were grown to $\text{OD}_{600} \sim 0.2$ and then pulsed with 2 mL of a 5.25 g/L $\text{U-}^{13}\text{C}$ phenol stock solution for a final labeled phenol concentration of ~ 0.5 g/L. The cultures were quenched at 1 minute using the Fast-Cooling procedure (Hollinshead et al., 2016; Abernathy et al., 2017). To study the effect of benzoate on phenol utilization, 100 mL cultures with 0.5 g/L fully labeled phenol were grown to $\text{OD}_{600} \sim 0.35$, and then the labeled cultures were mixed with 1 mL of 20 g/L unlabeled benzoate. After the benzoate pulse, time course samples from the culture were quenched at 20 seconds, 10 minutes, and 3 hours.

At each metabolite quenching time, ~ 10 mL of culture was poured into ice cold carbon-free media B, and then placed into a liquid nitrogen bath. The samples were stirred briefly and then centrifuged (8000 g) at $0\text{ }^\circ\text{C}$ for 5 minutes. The pellets were stored at $-80\text{ }^\circ\text{C}$ until metabolite extraction. To determine labeling in free metabolites, cell pellets were resuspended in 1 mL of 7:3 methanol:chloroform, and shaken at 250 rpm at $4\text{ }^\circ\text{C}$ for 6 hours with hourly vortexing. The methanol layer was separated by the addition of 500 μL water followed by centrifugation after which the aqueous layer was collected. This separation process was repeated twice. The collected samples were frozen at $-80\text{ }^\circ\text{C}$, then lyophilized at $-50\text{ }^\circ\text{C}$. The samples were reconstituted with water and analyzed using an Ion Pairing LC-MS method at the Donald Danforth Plant Science Center (Creve Coeur, MO, USA) (Abernathy et al., 2017). To measure metabolite pool size, an isotope ratio approach was used (Bennett et al., 2008; Abernathy et al., 2017). More specifically, *E. coli* was grown on $\text{U-}^{13}\text{C}$ glucose to produce fully-labeled internal standards for each metabolite, while *R. opacus* culture was grown on unlabeled substrates. The cultures were quenched and mixed together at a 1:1 biomass content ratio for metabolite extraction and LC-MS measurements. The relative metabolite pool size was calculated based on ^{13}C ratios.

2.4. Flux calculations

Steady-state flux analysis calculations were done using the software INCA (Isotopomer Network Compartmental Analysis) (Young, 2014). The basis of the *R. opacus* flux model is the KEGG genome annotation, including the β -ketoadipate pathway, the TCA cycle, the anaplerotic reactions, glycolysis, and the EDP. Carbon mappings for both ortho and meta pathways are shown in Supplemental Fig. 1. The *R. opacus* central flux network is largely similar to the model bacterial species *E. coli* with major differences in the inclusion of phenol \rightarrow acetyl-CoA + succinyl-CoA, a modified biomass equation (Crown et al., 2015), and the reversibility of glycolysis and the EDP to allow for gluconeogenesis. Labeling data of key proteinogenic amino acids, biomass growth, and

substrate consumption rate were used for flux calculation. Based on measurement errors from parallel labeling experiments, 90% confidence intervals of fluxes were calculated via INCA's parameter continuation function (See supplementary Excel file for metabolic reactions, flux constraints, amino acid labeling fitting, and statistical analysis).

Flux balance analysis (FBA) of the central metabolic network was done using INCA to further compare actual metabolic fluxes with optimal flux topologies. In addition to maximizing biomass or fatty acid production, three other objective functions were tested with fixed biomass growth rate: maximizing NAD(P)H, ATP, or minimizing sum of fluxes (i.e., enzyme usage). The FBA results were compared to ^{13}C -MFA by the sum of squared residuals between optimal flux and measured flux in central pathways.

2.5. Biomass composition analyses and substrate/product concentration measurements

Cell cultures were grown to exponential phase, pelleted, washed with sterile water and then lyophilized. Amino acid composition analysis was performed by the Molecular Structure Facility, University of California (Davis, CA, USA). Fatty acid composition analysis was performed by Microbial ID (Newark, DE, USA). Overflow metabolites were analyzed using enzyme kits from R-Biopharm (Pfungstadt, Germany). Phenol and benzoate in the culture supernatant were derivatized using methyl chloroformate (Madsen et al., 2016) and quantified using a custom GC-MS-FID system (gas chromatography-mass spectrometry-flame ionization detector). Briefly, the culture supernatant was centrifuged at 16,000 g for 5 min, and 200 μL of the culture supernatant was mixed with 40 μL of 5.0% (w/w) sodium hydroxide solution, 200 μL of methanol, and 50 μL of pyridine. Methyl chloroformate (50 μL) was added to the mixture in two 25 μL aliquots. Next, 400 μL of chloroform containing a decane internal standard was added to the sample, followed by the addition of 400 μL of 50 mM sodium bicarbonate solution to induce phase separation of the aqueous and organic layers. Samples were vortexed between each step to ensure complete mixing. After phase separation, the organic phase was transferred to a GC vial with a 350 μL glass insert (Agilent), and samples were analyzed using an Agilent 7890A GC coupled to both an Agilent 5975C mass spectrometer containing a triple-axis detector and an Agilent G3461A FID detector with a methanizer (Activated Research Company; Eden Prairie, MN, USA). The Agilent 7890A GC was equipped with a Restek fused silica RTX-50 capillary column (30 m by 0.25 mm, 0.5 μm film thickness), and helium was used as the carrier gas. 1 μL of the organic phase was injected with a splitting ratio of 10:1 using the autosampler. For GC runs, the inlet was maintained at 250 $^{\circ}\text{C}$, and the oven was held for 2 min at 40 $^{\circ}\text{C}$, heated to 300 $^{\circ}\text{C}$ using a 5 $^{\circ}\text{C}/\text{min}$ ramp, and held at 300 $^{\circ}\text{C}$ for 5 min. All data was exported and analyzed using the Agilent ChemStation Software, and peak intensities were normalized to the decane internal standard. Phenol and benzoate were identified based on retention time and concentrations were determined using external standard curves.

2.6. RNA-seq analysis

Raw transcriptomic sequences were downloaded from the Sequence Read Archive (SRA) accession number SRP131196 (Henson et al., 2018a). Sequences were quality trimmed using Trimmomatic (Bolger et al., 2014) before mapping to the Chinese Academy of Science reference genome of *R. opacus* (ASM59954v1) (Chen et al., 2014) using Bowtie2 (Langmead and Salzberg, 2012). The resulting SAM files were converted to the BAM format and indexed using SAMtools (Li et al., 2009). Expression counts were then calculated using featureCounts (Liao et al., 2014) and normalized using DESeq2 (Love et al., 2014). Supplemental Table 1 summarizes RNA-seq data of *R. opacus* strains growing with glucose and phenol.

Table 1

A summary of the growth rate, corresponding doubling times (t_D), and maximum optical density of *R. opacus* on four different carbon substrates. All data presented is the average of biological triplicates \pm standard deviation.

Carbon Substrate	Growth Rate (hr^{-1})	t_D (hr)	Maximum OD_{600}
2.0 g/L Acetate	0.16 \pm 0.02	4.30	1.08 \pm 0.01
0.5 g/L Phenol	0.17 \pm 0.02	4.10	0.82 \pm 0.02
0.3 g/L Phenol + 1.0 g/L Glucose	0.24 \pm 0.01	2.96	1.53 \pm 0.01
1.0 g/L Glucose	0.25 \pm 0.02	2.81	1.20 \pm 0.02

3. Results and discussion

3.1. Cell growth and biomass composition

The glucose metabolism of *R. opacus* has been studied previously (Hollinshead et al., 2015). Here, we investigated the growth rates of *R. opacus* on acetate, phenol, phenol with glucose, and glucose (Table 1). The fastest growth rate (0.24 hr^{-1}) for wild type *R. opacus* was observed when glucose was the sole carbon source. Growth on phenol was, as expected, slower (0.17 hr^{-1} , $P = 0.013$; two-tailed Student's t -test), likely owing to a combination of its toxic effects and less efficient phenol degradation processes. When phenol is provided in combination with glucose, these disadvantages are largely mitigated – the rapidity with which glucose can be processed apparently compensated for the kinetic disadvantages of phenol metabolism (e.g., requirement of gluconeogenesis), which allowed the cultures to grow nearly as quickly as the glucose-only case ($P = 0.46$). Moreover, the co-utilization of both substrates produced more biomass at the end of the cultivations ($P < 0.01$). Interestingly, acetate-fed cultures showed similar growth performance to phenol-fed cultures ($P = 0.65$). The TCA cycle is the entering point of the central flux network for both acetate and phenol, but phenol utilization requires more conversion steps than acetate consumption. Therefore, the similar growth rates indicate that the β -ketoadipate pathway in *R. opacus* is as efficient as the acetate conversion route (acetate \rightarrow acetyl-CoA).

A biomass composition analysis was conducted on cultures grown in phenol, glucose, and a phenol-glucose mixture. The data from the phenol culture was used to modify the biomass equation in the metabolic flux model. Fig. 1A shows the proteinogenic amino acid composition of *R. opacus* from three tested samples, where glutamate/glutamine and alanine were most abundant. Proteinogenic amino acid synthesis in *R. opacus* undergoes minimal changes when grown on different carbon sources. *R. opacus* is known to store high concentrations of lipids in late growth phases, and reportedly can accumulate lipids up to 80% of its dry cell weight under low-nitrogen stress (Alvarez et al., 1996; Henson et al., 2018a). In the exponential growth phase when nitrogen was still available, ~ 0.3 g lipid per gram dry cell weight was accumulated in biomass samples. We further probed the fatty acid profiles of *R. opacus* when fed the three previously-described carbon sources with sufficient nitrogen (Fig. 1B). In general, the most abundant fatty acid (in the form of acyl groups of lipids) is palmitic acid (16:0), accounting for approximately 30% of total lipid fatty acids. Compared to the model bacterium *E. coli*, *R. opacus* contains higher proportions of long-chain fatty acids (Supplemental Fig. 2). Specifically, 47% of fatty acids in *R. opacus* were found to contain 17 carbons or more, whereas only 12% of fatty acids in *E. coli* have over 16 carbons (Neidhardt et al., 1990). Additionally, *R. opacus* natively produces C15 fatty acids and branched-chain fatty acids (BCFAs) containing 16, 17, and 18 carbon atoms. Unlike most Gram-positive bacteria and some engineered Gram-negative strains which only produce terminal BCFAs (Bentley et al., 2016; Jiang et al., 2015; Kaneda, 1966), *R. opacus*' BCFAs have internal branches, which are expected to produce biofuels with better cold-flow properties than terminally-branched fuels (Pond

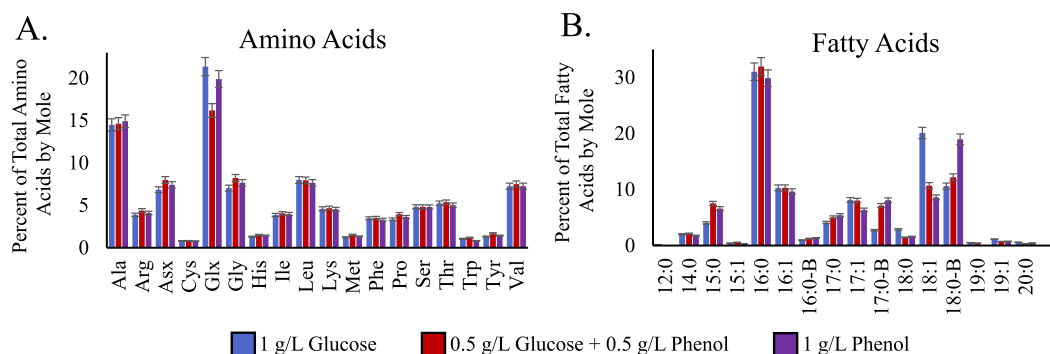


Fig. 1. The distribution of amino acids (A) and fatty acids (B) in *R. opacus* with three different carbon sources. Asx = aspartate/asparagine and Glx = glutamate/glutamine; fatty acids are denoted as carbon chain length:number of unsaturated bonds, with a B indicating branching. Error bars are estimates of technical uncertainty.

and Langworthy, 1987). The carbon source affected the abundance of some fatty acids. Notably, ~20% of the total fatty acids in phenol-fed culture were C18 BCFAs.

3.2. Phenol degradation via the β -ketoacid pathway

The enzymatic pathways to degrade aromatic substrates can be grouped into categories based on the position of bond cleavage (Fuchs et al., 2011). The KEGG annotation for *R. opacus* contains every gene for the meta cleavage of catechol, while one of the genes in the ortho pathway, 3-oxoadipate CoA-transferase, is unannotated. Both pathways begin with a two-component flavoprotein monooxygenase, phenol hydroxylase, which oxidizes the phenol ring to form catechol (Fig. 2). Saa et al. studied this enzyme in *Rhodococcus erythropolis* and found that it

can accept electrons from both NADH and NADPH to cleave O_2 molecules. However, phenol hydroxylase's affinity for NADH was measured to be 5–10 times greater than its affinity for NADPH (Saa et al., 2010). This may be an evolutionary adaptation to avoid competition for NADPH between phenol consumption and biomass formation. The ortho and meta pathways diverge with the ortho branch employing catechol-1,2-dioxygenase and the meta branch using catechol-2,3-dioxygenase. The intermediates in the ortho pathway include cis-cis-muconic acid and β -ketoacid, and its end products are acetyl-CoA and succinyl-CoA. In contrast, the meta pathway's intermediates include 2-hydroxymuconic semialdehyde, and its final products are pyruvate, formate, and acetyl-CoA (Sridevi et al., 2012). Meta-cleavage has been found in *Pseudomonas* species to degrade phenol and phenol derivatives (Kukor and Olsen, 1991). To determine which route is used by

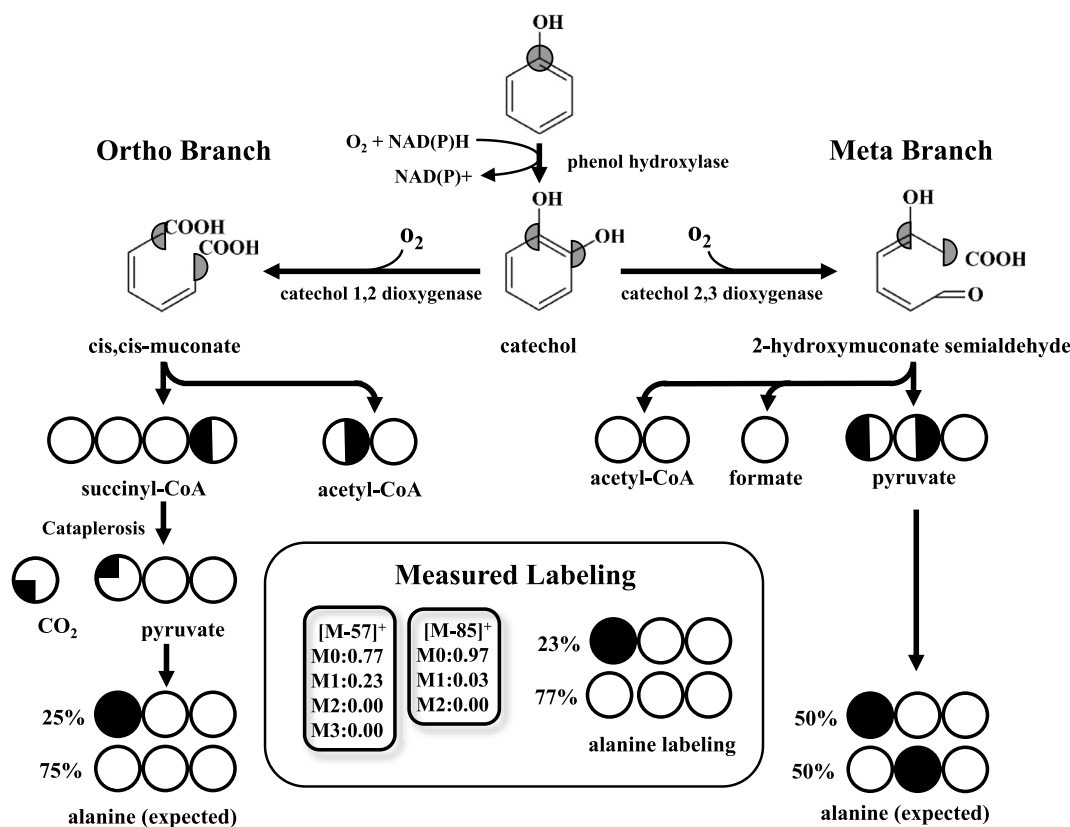


Fig. 2. $1\text{-}^{13}\text{C}$ phenol catabolism in *R. opacus* is through the ortho-cleavage. GC-MS data of alanine gives labeling data for pyruvate. The [M-57]⁺ and [M-85]⁺ fragments were used to determine the labeling of each carbon of pyruvate. The labeling of pyruvate closely matches the expected labeling for phenol catabolism through the ortho branch. A detailed tracing is shown in Supplemental Fig. 1.

R. opacus, we used 1-¹³C phenol labeling (Fig. 2). The symmetry of catechol results in two different alanine labeling patterns for each branch. In the ortho pathway, 50% of labeled carbon will end up as the 4th position carbon of succinyl-CoA and the remaining 50% will occupy the 1st position of acetyl-CoA. In the TCA cycle, succinyl-CoA is converted to succinate, another symmetric molecule. The reactions of cataplerosis, e.g., the phosphoenolpyruvate (PEP) carboxykinase-catalyzed reaction, release the 4th position carbon as CO₂, and convert the remaining 3-carbon fragment to pyruvate. The expected labeling pattern for pyruvate derived from the ortho branch is therefore 25% first-position labeled and 75% unlabeled. In contrast, the meta-cleavage will create pyruvate molecules with an even split between those labeled in the first and the second positions. Alanine's sole precursor is pyruvate, and thus pyruvate's labeling can be determined by measuring alanine. Our analysis showed that ~23% of alanine was labeled only at the 1st position, and ~77% of alanine was unlabeled. This provides strong evidence that the ortho pathway is the exclusive route for phenol degradation. The labeling result is consistent with our previous gene knockout analyses (Henson et al., 2018a). Specifically, when muconate cycloisomerase, an ortho pathway enzyme, was disrupted, *R. opacus* was unable to grow on phenol. Additionally, proteomic data from this species has shown that several enzymes in the ortho pathway are abundant during aromatic metabolism (Xie et al., 2019). The missing ortho pathway reaction (3-oxoadipate → 3-oxoadipyl CoA) could be catalyzed by succinyl-CoA:3-ketoacid-CoA transferase (PD630_RS25340 + PD630_RS25345) (Yoneda et al., 2016). We also found that the presence of formate (0.5 g/L) was inhibitory to cell growth, implying that the meta pathway with byproduct formate is unlikely to be beneficial for growth. It is worth noting that the genes coding the ortho pathway enzymes are found in two distinct clusters on the chromosome, while the genes for the meta pathway are scattered across the genome and two endogenous plasmids. All these analyses prove the value of ¹³C tracing to delineate functional pathways and to fill the annotation gaps.

3.3. *R. opacus* flux map

¹³C-MFA was performed to comprehensively investigate *R. opacus*' phenol metabolism (Fig. 3A). The metabolic model had 71 reactions and 33 independent parameters, and was constrained by 174 independent mass isotopomer measurements, resulting in 141 degrees of freedom. Amino acid labeling data with 0.75 mol % measurement error from parallel tracer experiments (1-¹³C Phenol and 2,6-¹³C Phenol) was used to generate the flux map. The SSR (sum of square residuals) for the presented fit was 119.4, which is inside the 90% confidence bounds for the SSR [114.6 169.7]. Experimentally, the rate of phenol uptake (i.e., the amount of phenol entering the central metabolism per cell mass within a given time) at exponential phase was measured to be 2.3 mmol/h/g dry cell weight (Supplemental Fig. 3). ¹³C-MFA shows that per 100 mmol of phenol consumed, ~2 mmol extracellular overflow metabolites (i.e., succinate), ~370 mmol CO₂, and ~220 mmol C of biomass (~4.7 g) were produced, resulting in a ~50% yield of biomass from phenol (Fig. 3A).

The TCA cycle of *R. opacus* in phenol culture has very high fluxes to sustain aerobic growth. The citrate entrance node has a relative flux over 100, which is much higher than reported fluxes in glucose-fed *E. coli* (Crowe et al., 2015). The direct infusion of succinyl-CoA from phenol degradation drives high fluxes through succinyl-CoA ligase, succinate dehydrogenase, and fumarate hydratase in the TCA cycle and causes succinate overflow (Supplemental Fig. 4). In the supernatant, α-ketoglutarate could also be detected while acetate secretion was not observed. The overflow of the TCA cycle works to balance excessive succinyl-CoA flux from phenol degradation. In contrast, excess acetyl-CoA (i.e., not forming citrate in the TCA cycle) enters into biomass pools (lipid and amino acids). Further, the glyoxylate shunt is measurable, offering an alternative route for acetyl-CoA consumption. On the other

hand, several anaplerotic reactions are also active to direct flux outside the TCA cycle (note: the confidence intervals of these fluxes are relatively wide due to limited labeling resolution). For instance, the malic enzyme is active to pump the TCA fluxes for pyruvate synthesis. Moreover, both ¹³C-MFA and gene expression data identified the GTP-dependent PEP carboxykinase (PD630_RS08140) as the driving force for gluconeogenesis (OAC→PEP) and flux towards the upper pathways (the ED pathway and the pentose phosphate pathways). Interestingly, the model shows that the EDP, operating in reverse, can serve as a secondary route to the upper pathways. Fluxes in the upper pathways of phenol-fed cultures are small and primarily used for biomass synthesis.

To offer a deeper understanding of *R. opacus* flux network optimality, the ¹³C-MFA model was compared to flux balance analysis results using five different objective functions (Supplemental Fig. 5) (Schuetz et al., 2007). Based on the SSRs between the MFA fluxes and FBA fluxes, the metabolism of *R. opacus* is most closely optimized to maximize the production of energy molecules rather than the production of biomass or fatty acids or the minimization of enzyme use (Supplemental Fig. 6). The high TCA cycle fluxes elucidated by ¹³C-MFA facilitate NADH, and subsequently ATP production. The elevated priority of energy molecules is the tradeoff against biomass growth when growing on stress-inducing aromatic substrates. Moreover, *R. opacus* flux topology is not geared towards minimal usage of enzymes, allowing for metabolic flexibility to utilize unconventional substrates.

3.4. Cofactor balance and energy metabolism

Phenol metabolism carries very low fluxes through the oxidative pentose phosphate pathway, which is the major NADPH source for common glucose-utilizing microbes (such as *E. coli*). Instead, significant TCA fluxes are responsible for generating large amounts of NADH, NADPH, and ATP (Fig. 3B). Unlike NADPH, which is primarily consumed in the formation of biomass, NADH is used for the oxidation of phenol to catechol and the production of ATP. *R. opacus* can use NAD-dependent malic enzyme (PD630_RS12555, EC 1.1.1.38), but lacks NADP-dependent malic enzyme (EC 1.1.1.40). Consequently, most NADPH generation occurs in the TCA cycle by NADPH-dependent isocitrate dehydrogenase (PD630_RS13780), which explains the necessity to maintain high flux through the TCA cycle. A search of *R. opacus*'s genome identified NAD(P) transhydrogenase subunits alpha and beta (PD630_RS39815 and PD630_RS39805). The transhydrogenase might further fine-tune the cofactor balance. On the other hand, ATP can be generated directly by the TCA cycle (as GTP) and indirectly through oxidative phosphorylation. ATP is needed mainly for biomass formation (in particular for lipid synthesis) and other cellular processes (e.g., cell maintenance, substrate active transport, and gluconeogenesis). Additionally, we calculated the intracellular energy charge based on LC-MS measurements to determine the relative concentrations of ATP, ADP, and AMP ($Energy\ Charge = \frac{[ATP] + \frac{1}{2}[ADP]}{[ATP] + [ADP] + [AMP]}$) (Supplemental Fig. 7). Phenol-fed cultures have an energy charge of ~0.9, indicating that the concentration of ATP is much greater than that of ADP and AMP combined. Glucose-fed cultures have a comparable energy charge (~0.85). An explanation for this similarity is that, during aerobic growth, the NADH synthesized from either substrate can be effectively used via oxidative phosphorylation to generate ATP (Fig. 3B). These results along with FBA results demonstrate that *R. opacus* has sufficient energy-carrying molecules to support the production of high-energy biofuels from different feedstocks.

3.5. RNA-seq analysis of flux network

RNA-seq was used to compare transcriptional regulation between conditions (Fig. 3, Supplemental Table 1). It is important to note that while transcriptomics can illuminate how genes are regulated, it does not strictly correlate to enzyme activities or flux values due to

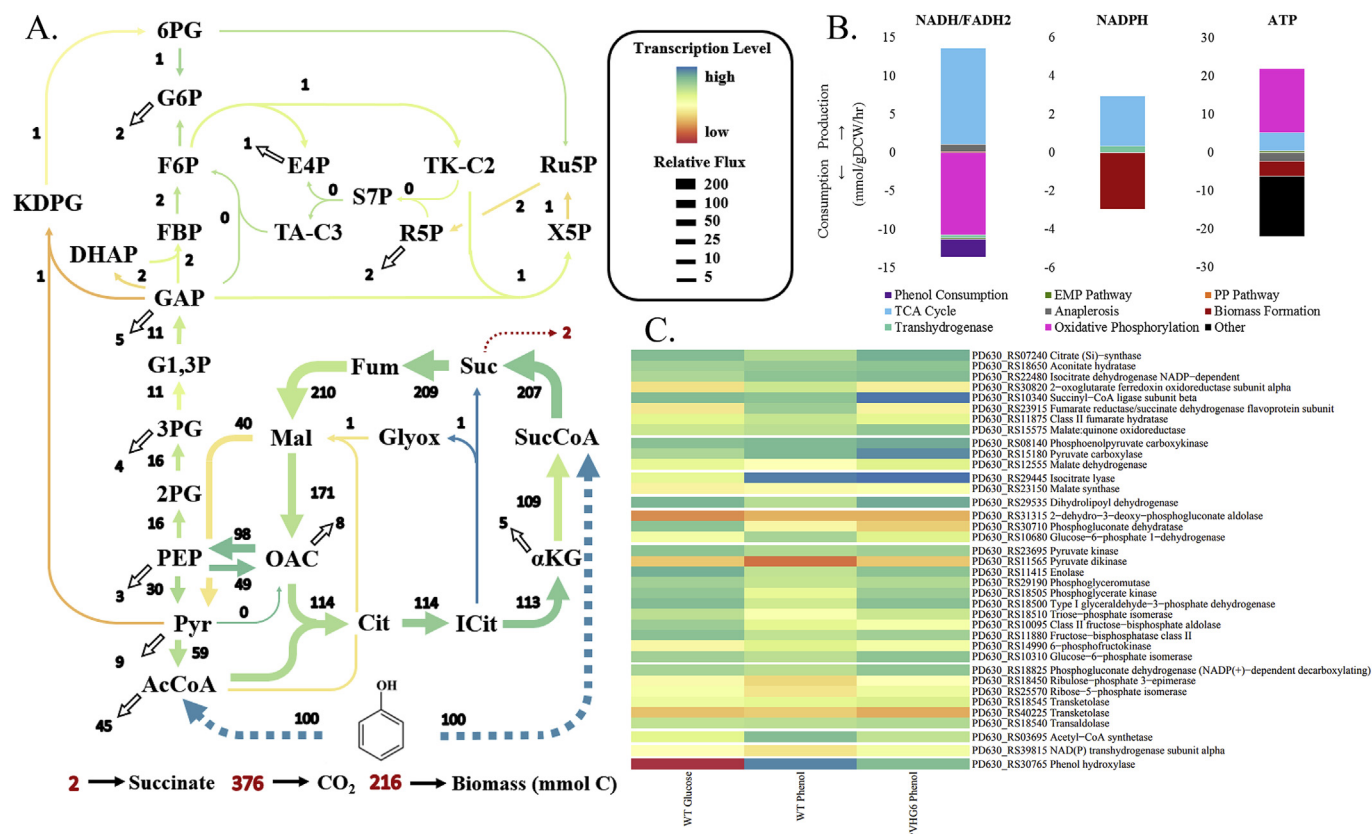


Fig. 3. Flux and transcriptional analyses of *R. opacus* strains. (A) *R. opacus* PD630's flux map when phenol is the sole carbon source. The flux values are relative flux distributions based on 100 mmol of phenol consumed by the cell to generate 100 mmol of influx toward both acetyl-CoA and succinyl-CoA. Arrow color corresponds to the relative gene expression levels of the enzyme that catalyzes the reaction (yellow/orange = low and green/blue = high). Arrow size corresponds to relative flux. White arrows are fluxes to biomass formation. The dashed red arrow is flux out of the cell. (B) The major sources and sinks of NADH, NADPH, and ATP in *R. opacus*'s phenol metabolism. (C) The transcript levels from wild type and an adapted strain (PVHG6) of *R. opacus* grown on glucose or phenol were compared for the following metabolisms: TCA cycle, anaplerotic pathways, the glyoxylate shunt, the ED pathway, the EMP pathway, the pentose phosphate pathway, transhydrogenation, and phenol consumption (Henson et al., 2018a). (For interpretation of the references to color in this figure legend, the reader is referred to the Web version of this article.)

variations in translational rate and allosteric regulation. Using data generated in the previous report, we compared the transcription levels of central pathway enzymes in glucose- and phenol-fed cultures of wild type *R. opacus* and *R. opacus* PVHG6, a mutant strain which was adaptively evolved for improved growth on a mixture of aromatic compounds (Fig. 3C) (Henson et al., 2018a). When consuming glucose, *R. opacus* expressed phenol hydroxylase at low levels, while its key enzymes for glycolysis are mostly highly expressed. During phenol utilization, *R. opacus*' isocitrate lyase (PD630_RS29445) was highly expressed, but the glyoxylate shunt flux was low.

Glucconeogenesis, which is required when phenol is the sole carbon source, is typically thought to occur exclusively through the EMP pathway operating in reverse. However, the ¹³C-MFA model suggests that the EDP enzymes (in the reverse direction) also play a role in *R. opacus*. Transcriptomic data was used to investigate this finding. Despite its low transcription levels in glucose cultures, the EDP was found to be the main route for glucose consumption in *R. opacus* (Hollinshead et al., 2015). The EDP has comparable transcription levels in phenol-fed cultures and glucose cultures, and this suggests that it is active in the reverse direction when phenol is the carbon source. When running in reverse, the EMP pathway uses most of the same enzymes as it does when it runs forward, with the exception of conversion between FBP to F6P and pyruvate to phosphoenolpyruvate (PEP). In the glycolytic direction, F6P is converted to FBP by 6-phosphofructokinase (PD630_RS14990); in the glucconeogenic direction, FBP → F6P occurs via fructose-1,6-bisphosphatase (PD630_RS11880). Interestingly, the number of transcripts of fructose-1,6-bisphosphatase is lower in phenol

cultures than in glucose cultures (Supplemental Table 1), implying fructose-1,6-bisphosphatase activity is reduced during phenol metabolism. Additionally, the gene encoding pyruvate dikinase (PD630_RS11565, pyruvate → PEP) has very low expression levels during phenol metabolism. Therefore, the anaplerotic reaction via phosphoenolpyruvate carboxykinase (PD630_RS08140, oxaloacetate → PEP) is indispensable for supporting gluconeogenic fluxes. Intriguingly, the aromatic-mixture-adapted strain PVHG6, was found to express pyruvate dikinase and succinyl-CoA ligase at higher rates than the wild type in phenol culture, which may facilitate aromatic utilization and tolerance.

3.6. Pulse-trace labeling and metabolite pool measurement

The glucconeogenesis pathways were further investigated with a ¹³C-pulse experiment (Fig. 4A and 4B, Supplemental Fig. 8). Conceptually, metabolites with the highest flux are expected to incorporate ¹³C carbon most rapidly. The labeling order of glycolysis metabolites observed in phenol-fed cultures is the reverse of that in glucose-fed metabolism: phosphoenolpyruvate (PEP) was labeled first, followed closely by 3-phosphoglycerate (3PG). Fructose-bis-phosphate (FBP) was found to be labeled significantly faster than fructose-6-phosphate (F6P) ($P = 0.03$). This may be due to a combination of the thermodynamic barrier between FBP and F6P (i.e., reaction Gibbs free energy favors flux from F6P to FBP), the small pool size of FBP (Fig. 4C), and the low transcription levels of fructose-1,6-bisphosphatase (Fig. 3C, Supplemental Table 1).

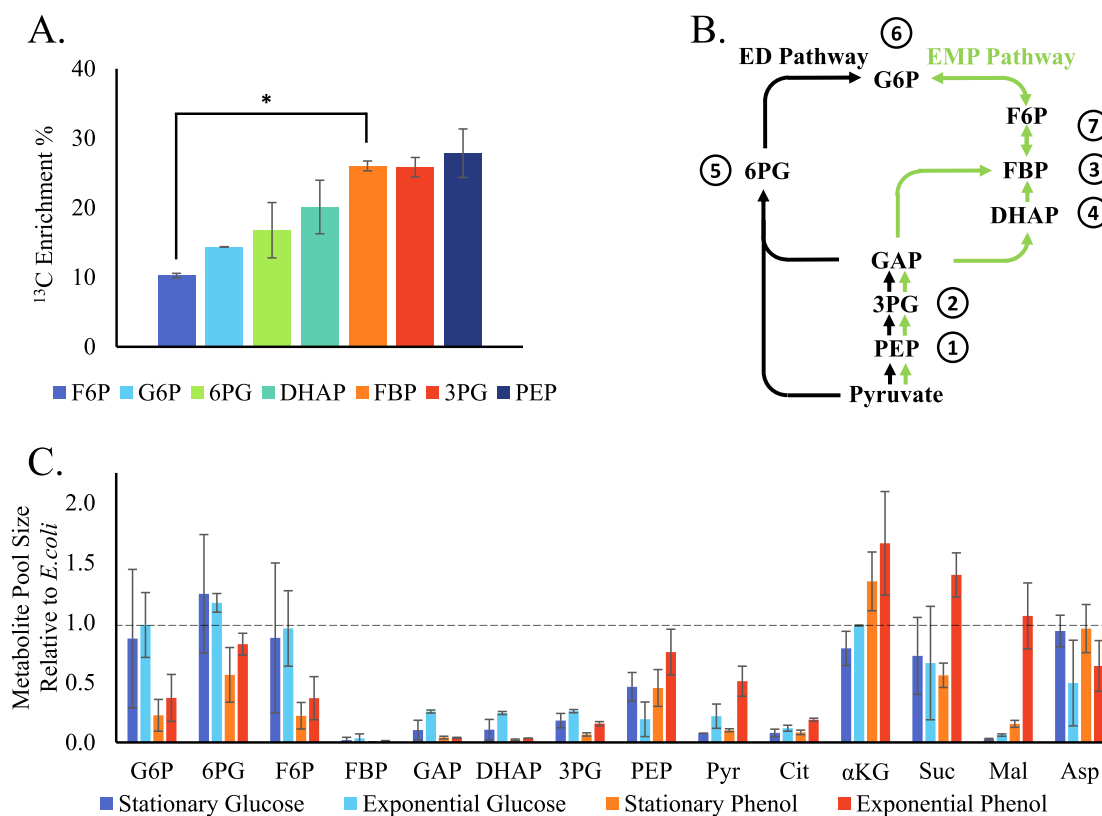


Fig. 4. Dynamic labeling and metabolite pool size measurement. (A) Pulse-trace labeling data from cultures that were quenched within 1 min after ^{13}C phenol was added. Asterisk (*) indicates that the difference between F6P and FBP values is statistically significant ($P < 0.05$, one mean, two-tailed Student's t-test). (B) A simplified metabolic map of the ED and EMP pathways annotated with 1 being the fastest labeled metabolite and 7 being the slowest. (C) Intracellular metabolite concentrations relative to those in glucose-fed *E. coli* (used as internal standards).

The intracellular metabolite concentrations, or pool sizes, of *R. opacus* cultures grown on glucose and phenol were measured at stationary and exponential time points (Fig. 4C). Cells growing exponentially on phenol have very high quantities of TCA cycle intermediates. However, their intracellular concentrations of fructose-bisphosphate (FBP), dihydroxyacetone phosphate (DHAP), and glyceraldehyde-3-phosphate (GAP) are lower than 10% of those of *E. coli*. This offers thermodynamic evidence for high TCA cycle fluxes paired with low reverse EDP and gluconeogenic fluxes. Compared to glucose-fed *E. coli*, phenol-fed *R. opacus* has relatively low citrate concentrations. This may be the result of a highly active isocitrate dehydrogenase, an enzyme needed for both αKG and NADPH production. Also, *R. opacus* has relatively high concentrations of α -ketoglutarate (αKG), especially during exponential growth. An explanation is that succinyl-CoA/succinate accumulation from phenol degradation inhibits α -ketoglutarate dehydrogenase ($\alpha\text{KG} \rightarrow$ succinyl-CoA), leading to excess amounts of αKG (note: both succinate and αKG were detected in the supernatant). Therefore, succinyl-CoA is likely a bottleneck node causing metabolite overflow during phenol metabolism.

3.7. Phenol co-utilization with other substrates

Industrial applications of *R. opacus* will require growth on lignin hydrolysates, which contain a heterogeneous mixture of compounds (Beckham et al., 2016). Notably, *R. opacus* can consume aromatic compounds simultaneously with glucose without exhibiting catabolite repression (Hollinshead et al., 2015). However, it was found that *R. opacus* consumes some aromatic compounds sequentially, rather than concurrently (Henson et al., 2018a). Here we further investigated co-metabolism of phenol with competing substrates (glucose, acetate, succinate, and benzoate) (Fig. 5A, 5B, 5C). Our findings for phenol-

glucose cultures are consistent with the previous report, finding no interaction between the two substrates. A separate study observed that phenol degradation enzyme transcripts in *Rhodococcus erythropolis* CCM2595 were downregulated in the presence of succinate (Szököl et al., 2014). Yet, when phenol and succinate were co-fed to *R. opacus* in our experiment, cells predominantly used phenol (> 90% of carbon originated from phenol). Since phenol metabolism produces excessive succinate, *R. opacus* may repress the utilization of external succinate in order to preferentially consume the toxic compound. Similarly, *R. opacus* can co-utilize phenol and acetate, and phenol is preferred (~70% of proteinogenic carbon originated from phenol). On the other hand, benzoate was found to be utilized faster than phenol (Fig. 5B, 5C).

Three experiments were performed to elucidate the interaction of phenol and benzoate. In the first experiment, amino acid labeling was used to quantify the relative uptake rate between benzoate and phenol (Fig. 5B). We found that the ratio of benzoate/phenol uptake rate (calculated via ^{13}C labeling data) during early growth phase showed a linear relation to the concentration ratio of the two substrates in the media (Supplemental Fig. 9). When cells grew in media containing equal moles of fully labeled phenol and unlabeled benzoate, the proteinogenic amino acids contained ~90% ^{12}C carbon from benzoate. This result indicates that the wild type strain consumes both substrates, but its benzoate utilization is much faster than its phenol utilization. The second experiment examined how the concentrations of benzoate and phenol in the media decreased over time (Fig. 5C). We validated that benzoate serves as the main carbon source when both benzoate and phenol are present: phenol was consumed slowly in the presence of benzoate, and its consumption increased once benzoate was nearly exhausted. In the final experiment, a benzoate pulse was given into fully-labeled phenol-fed, exponentially growing cultures to investigate

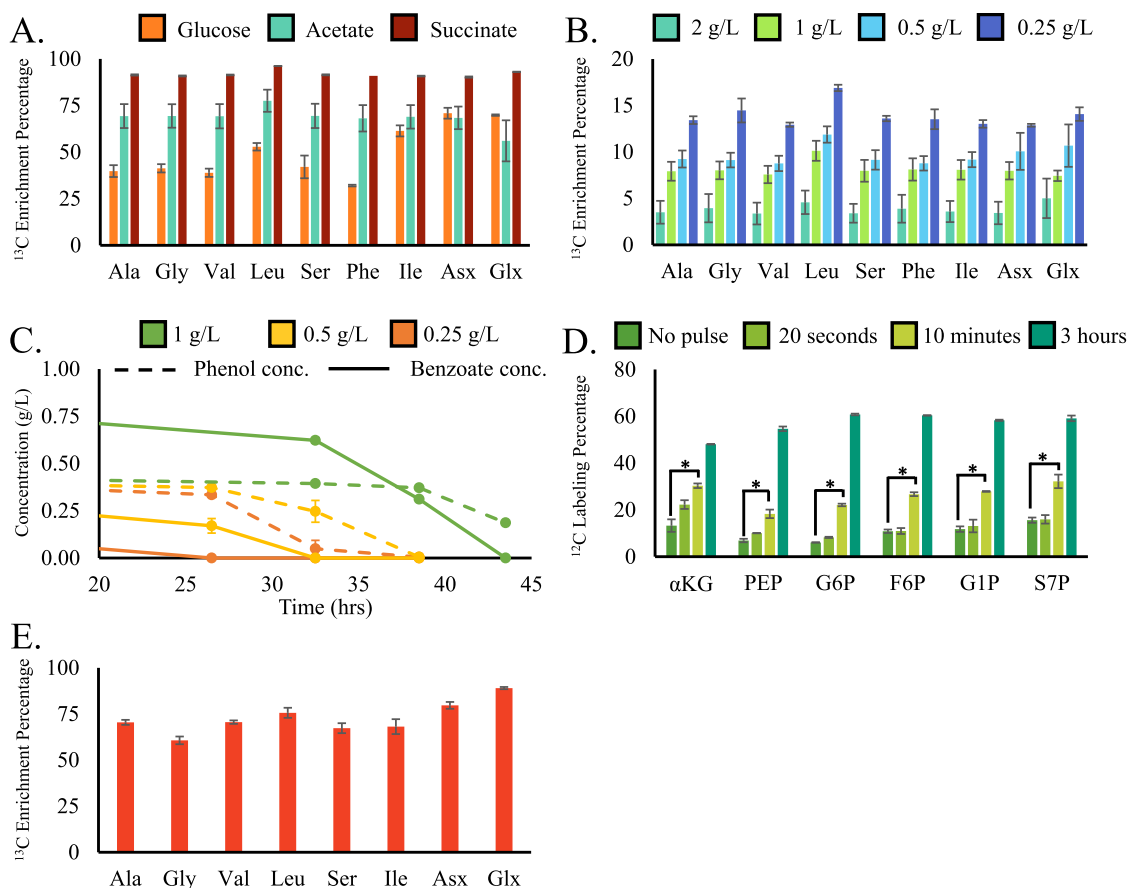


Fig. 5. Mixotrophic phenol metabolism. (A) The contribution of phenol-derived carbon to amino acids in the presence of 0.5 g/L U-¹³C phenol and 1 g/L of unlabeled glucose, acetate, or succinate. Samples were taken at early exponential growth ($OD_{600} = 0.4\text{--}0.5$) when both substrates remained in the media. (B) The contribution of phenol to the production of amino acids in the presence of 0.5 g/L U-¹³C phenol and decreasing concentrations of unlabeled benzoate. Samples were taken at early exponential growth phase ($OD_{600} = 0.25\text{--}0.3$) when both substrates remained in the media. The bars correspond to the relative uptake rate of phenol compared to that of benzoate. (C) The supernatant concentrations of phenol and benzoate over time when the starting concentration of U-¹³C phenol was 0.5 g/L and the starting concentration of benzoate was varied. (D) The contribution of benzoate-derived carbon to central metabolites at 20 seconds, 10 minutes, and 3 hours after a benzoate pulse into phenol-fed cultures. Asterisk (*) indicates that the difference between labeling is statistically significant ($P < 0.05$, one mean, two-tailed Student's t-test) (E) The contribution of acetate to amino acids in the presence of 1 g/L U-¹³C acetate and 1 g/L unlabeled succinate. Fig. 5A, 5B, 5C, and 5D represent data from biological duplicates. Fig. 5E represents data from technical triplicates.

the rate at which unlabeled benzoate enters into the central metabolism of *R. opacus* (Fig. 5D). To consider the contribution of CO₂ fixation to the unlabeled carbon percentage (Hollinshead et al., 2015), we included no-pulse controls with which the benzoate-pulsed cultures were compared (using one mean, two-tailed Student's t-test). When the phenol-growing *R. opacus* was quenched within 20 s of a benzoate pulse, only very small quantities of carbon from benzoate had entered the central metabolism (e.g., P values = 0.109, 0.052, and 0.014 for α KG, PEP, and G6P, respectively). In contrast, at 10 min, a significant amount of carbon had been incorporated into central metabolites from the added benzoate ($P < 0.05$ for α KG, PEP, and G6P), which indicates that phenol catabolism in *R. opacus* can quickly shift to benzoate utilization without a long lag phase.

The downstream products of phenol are acetyl-CoA and succinyl-CoA. To investigate how these two substrates interact, we grew *R. opacus* in media containing fully-labeled acetate and unlabeled succinate (1 g/L each) (Fig. 5E). We hypothesized that acetate would be preferred over succinate because succinate is not fully consumed in phenol metabolism. GC-MS measurements indicates that *R. opacus* prefers acetate, as the carbon in its amino acids was mostly derived from acetate (~70%). This observation further confirmed that the succinate/succinyl-CoA metabolite nodes might comprise the rate-limiting steps during phenol metabolism, leading to flux congestion.

3.8. Mutant flux network after adaptive evolution

In a previous report, *R. opacus* was adaptively evolved to tolerate high concentrations of various aromatic compounds, including phenol, benzoate, vanillate, 4-hydroxybenzoate, and guaiacol (Henson et al., 2018a). Three mutant strains (P1, B2, and PVHG6) were obtained via adaptive evolution on increasing concentrations of phenol (P; up to 1.5 g/L), benzoate (B; up to 12.6 g/L), or a mixture of phenol, vanillate, 4-hydroxybenzoate, and guaiacol (PVHG; up to 3.0 g/L of total aromatics), respectively. These mutant strains were found to have distinct mutations and different growth profiles when provided with a mixture of phenol, vanillate, 4-hydroxybenzoate, guaiacol, and benzoate as a carbon source. To determine whether these mutations altered flux through central pathways, these evolved strains were grown on 0.5 g/L of 1-¹³C phenol (a low, permissive concentration for the wild type strain growth), and the resulting amino acid labeling patterns were compared to that of the wild type strain (Fig. 6). Adapted stains, P1 and PVHG6 showed similar growth rates on phenol as that of the wild type ($P = 0.70$ and $P = 0.11$, respectively) (Supplemental Table 2). The benzoate-adapted strain showed reduced growth on phenol compared to the wild type strain, only reaching an OD_{600} value of 0.2 after 50 h ($P = 3.7 \times 10^{-5}$), and a maximum growth rate of 0.10 hr^{-1} ($P = 0.01$). This supports previous findings that while adaptive

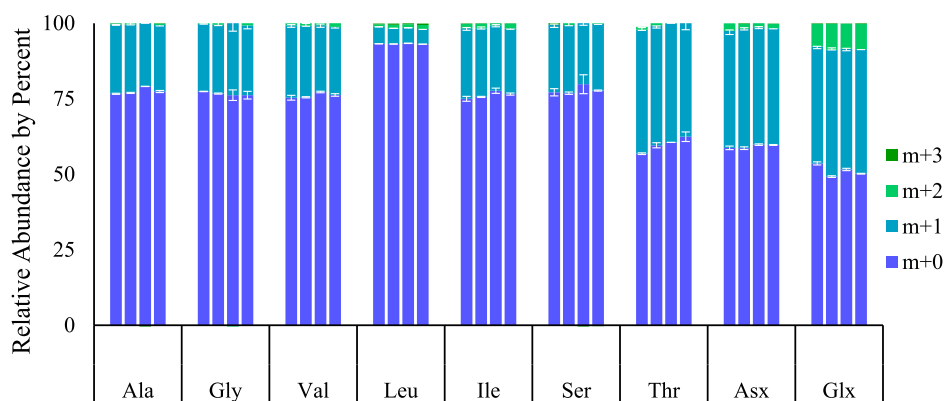


Fig. 6. The amino acid labeling pattern of wild type *R. opacus* and three mutant strains when grown on $1\text{-}^{13}\text{C}$ phenol (From left to right: wild type, phenol-adapted strain P1, benzoate-adapted strain B2, and aromatic-mixture-adapted strain PVHG6; $m + n$ = unlabeled mass m plus n labeled carbons).

evolution can help improve specific microbial traits, its untargeted nature can result in unexpected negative consequences or tradeoffs in other traits (Yi and Dean, 2016). Despite the growth defect in the benzoate-adapted strain, all three adapted strains produced amino acid labeling similar to the wild type, where the variances in labeling data were generally less than 2% (suggesting the invariability of relative flux distributions for biomass synthesis). This provides evidence that substrate adaptive evolution did not rewire the central flux network, which is a testament to the rigidity of the flux network (Long et al., 2017).

4. Conclusion and perspectives

Recently, non-model organisms have been gaining attention for addressing challenges in bio-manufacturing from renewable feedstocks (Czajka et al., 2017). Researchers can leverage the innate metabolic strengths of non-model species, including their tolerance to and utilization of toxic lignin-derived aromatics. However, rational strain engineering, which is routine practice with model organisms, cannot be applied to non-model strains until the complex metabolic networks of these microbes are better understood. In this work, we analyzed the aromatic metabolism in *R. opacus*, one of the most promising non-model organisms for lignin bioconversion, using a concerted systems biology approach. Importantly, this is the first reported ^{13}C -metabolic flux analysis completed in any organism using phenol as the sole carbon source. This study also shows that ^{13}C tracing is a powerful tool to precisely elucidate functional pathways with annotation gaps and to determine the time-scale of metabolic responses. Moreover, we established key links between the transcriptome, metabolome, and fluxome of this organism, and uncovered or confirmed some of its mechanisms for aromatic utilization.

By detailing *R. opacus*' metabolic network, this work offers guidelines for developing this species as a bio-manufacturing host. First, phenol-fed *R. opacus* shows strong fluxes through its TCA cycle. Thus, this host is ideal for producing chemicals derived from TCA cycle intermediates (e.g., acetyl-CoA and α -ketoglutarate). In contrast, its fluxes from phenol through gluconeogenesis are small, making it undesirable for the production of chemicals derived from sugar phosphates. Second, we investigated the carbon source utilization hierarchy of *R. opacus*. Interestingly, this strain utilizes glucose and phenol simultaneously without catabolite repression, preferentially consumes a toxic aromatic compound (phenol) over succinate and acetate, and uses benzoate faster than phenol. Since lignocellulosic degradation products are mixtures of compounds, *R. opacus*' co-utilization patterns will help to develop predictive metabolic models as well as guide future metabolic engineering efforts toward more-efficient conversion of lignocellulose to biofuels and biochemicals. Combining our findings from this work with our previous reports (Hollinshead et al., 2015; Henson et al., 2018a, 2018b; Yoneda et al., 2016), we are developing a genome-

scale metabolic model that enables prediction of metabolic fluxes for diverse carbon sources. Quantitative flux profiles obtained through ^{13}C -MFA provide an accurate description of internal metabolism that is invaluable when deciding future metabolic engineering approaches. For example, these flux profiles can be used in conjunction with methods like ROOM or MOMA to predict the effect of knockouts on metabolism and to offer computer-aided strain design (Martín et al., 2015; Ando and Martín, 2018). Third, ^{13}C analysis of the adaptively-evolved strains shows that their genetic differences do not lead to different flux networks. Recently, reliable genetic parts and engineering tools have been developed for *R. opacus*, allowing for gene expression control and genome modification in this strain (DeLorenzo et al., 2017; DeLorenzo et al., 2018). Future work will investigate how model-guided perturbations of its metabolism (e.g., knockouts and overexpression), as opposed to adaptive evolution, affects *R. opacus*'s flux network. With the ^{13}C -MFA model and detailed information regarding *R. opacus*' metabolic network provided from this work, future metabolic engineering efforts will be prediction-driven, speeding up its development as a bio-manufacturing host.

Data availability

1. Supplemental tables and figures.
2. Flux model construction and isotopomer data.

Acknowledgement

This project is supported by the US DOE (DE-SC0018324). For LC-MS services, the Donald Danforth Plant Science Center QTRAP LC-MS/MS acquisition was supported by National Science Foundation Grant DBI-1427621. We would like to thank Dr. Mary Abernathy for her help with sample preparation and data analysis of LC-MS experiments.

Abbreviations

3PG	3-phosphoglycerate
6PG	6-phosphogluconate
AcCoA	acetyl-CoA
α KG	α -ketoglutarate
Asx	aspartate and asparagine
Cit	citrate
DHAP	dihydroxyacetone phosphate
E4P	erythrose-4-phosphate
Fum	fumarate
F6P	fructose-6-phosphate
FBP	fructose-1,6-bisphosphate
G1P	glucose-1-phosphate
G1,3P	glycerate-1,3-phosphate

G2P	glycerate-2-phosphate
G6P	glucose-6-phosphate
GAP	glyceraldehyde-3-phosphate
Glx	glutamate and glutamine
ICit	isocitrate
KDPG	2-dehydro-3-deoxy-phosphogluconate
Mal	malate
OAC	oxaloacetate
PEP	phosphoenolpyruvate
Pyr	pyruvate
R5P	ribose-5-phosphate
Ru5P	ribulose-5-phosphate
Suc	succinate
SucCoA	succinyl-CoA
TA-C3	3-carbon fragment transferred by transaldolase
TK-C2	2-carbon fragment transferred by transketolase
X5P	xylulose-5-phosphate

Appendix A. Supplementary data

Supplementary data to this article can be found online at <https://doi.org/10.1016/j.ymben.2019.06.013>.

References

- Abdelaziz, O.Y., Brink, D.P., Prothmann, J., Ravi, K., Sun, M., García-Hidalgo, J., Sandahl, M., Hultheberg, C.P., Turner, C., Lidén, G., Gorwa-Grauslund, M.F., 2016. Biological valorization of low molecular weight lignin. *Biotechnol. Adv.* 34, 1318–1346.
- Abernathy, M.H., Yu, J., Ma, F., Liberton, M., Ungerer, J., Hollinshead, W.D., Gopalakrishnan, S., He, L., Maranas, C.D., Pakrasi, H.B., Allen, D.K., Tang, Y.J., 2017. Deciphering cyanobacterial phenotypes for fast photoautotrophic growth via isotopically nonstationary metabolic flux analysis. *Biotechnol. Biofuels* 10, 273.
- Alvarez, H., Mayer, F., Fabritius, D., Steinbüchel, A., 1996. Formation of intracytoplasmic lipid inclusions by *Rhodococcus opacus* strain PD630. *Arch. Microbiol.* 165, 377–386.
- Ando, D., García Martín, H., 2019. Genome-scale ¹³C fluxomics modeling for metabolic engineering of *Saccharomyces cerevisiae*. *Microbial Metabolomics. Methods Mol. Biol.* 1859, 317–345.
- Beckham, G.T., Johnson, C.W., Karp, E.M., Salvachua, D., Vardon, D.R., 2016. Opportunities and challenges in biological lignin valorization. *Curr. Opin. Biotechnol.* 42, 40–53.
- Bennett, B.D., Yuan, J., Kimball, E.H., Rabinowitz, J.D., 2008. Absolute quantitation of intracellular metabolite concentrations by an isotope ratio-based approach. *Nat. Protoc.* 3, 1299–1311.
- Bentley, G.J., Jiang, W., Guamán, L.P., Xiao, Y., Zhang, F., 2016. Engineering *Escherichia coli* to produce branched-chain fatty acids in high percentages. *Metab. Eng.* 38, 148–158.
- Boerjan, W., Ralph, J., Baucher, M., 2003. Lignin biosynthesis. *Annu. Rev. Plant Biol.* 54, 519–546.
- Bolger, A.M., Lohse, M., Usadel, B., 2014. Trimmomatic: a flexible trimmer for Illumina sequence data. *Bioinformatics* 30, 2114–2120.
- Chen, Y., Ding, Y., Yang, L., Yu, J., Liu, G., Wang, X., Zhang, S., Yu, D., Song, L., Zhang, H., Zhang, C., Huo, L., Huo, C., Wang, Y., Du, Y., Zhang, H., Zhang, P., Na, H., Xu, S., Zhu, Y., Xie, Z., He, T., Zhang, Y., Wang, G., Fan, Z., Yang, F., Liu, H., Wang, X., Zhang, X., Zhang, M.Q., Li, Y., Steinbüchel, A., Fujimoto, T., Cichello, S., Yu, J., Liu, P., 2014. Integrated omics study delineates the dynamics of lipid droplets in *Rhodococcus opacus* PD630. *Nucleic Acids Res.* 42, 1052–1064.
- Chubukov, V., Uhr, M., Le Chat, L., Kleijn, R.J., Jules, M., Link, H., Aymerich, S., Stelling, J., Sauer, U., 2013. Transcriptional regulation is insufficient to explain substrate-induced flux changes in *Bacillus subtilis*. *Mol. Syst. Biol.* 9, 709.
- Crown, S.B., Long, C.P., Antoniewicz, M.R., 2015. Integrated ¹³C-metabolic flux analysis of 14 parallel labeling experiments in *Escherichia coli*. *Metab. Eng.* 28, 151–158.
- Czajka, J., Wang, Q., Wang, Y., Tang, Y.J., 2017. Synthetic biology for manufacturing chemicals: constraints drive the use of non-conventional microbial platforms. *Appl. Microbiol. Biotechnol.* 101, 7427–7434.
- DeLorenzo, D.M., Henson, W.R., Moon, T.S., 2017. Development of chemical and metabolite sensors for *Rhodococcus opacus* PD630. *ACS Synth. Biol.* 6, 1973–1978.
- DeLorenzo, D.M., Rottinghaus, A.G., Henson, W.R., Moon, T.S., 2018. Molecular toolkit for gene expression control and genome modification in *Rhodococcus opacus* PD630. *ACS Synth. Biol.* 7, 727–738.
- Fuchs, G., Boll, M., Heider, J., 2011. Microbial degradation of aromatic compounds — from one strategy to four. *Nat. Rev. Microbiol.* 9, 803.
- Gani, A., Naruse, I., 2007. Effect of cellulose and lignin content on pyrolysis and combustion characteristics for several types of biomass. *Renew. Energy* 32, 649–661.
- García Martín, H., Kumar, V.S., Weaver, D., Ghosh, A., Chubukov, V., Mukhopadhyay, A., Arkin, A., Keasling, J.D., 2015. A method to constrain genome-scale models with ¹³C labeling data. *PLoS Comput. Biol.* 11, e1004363.
- Henson, W.R., Campbell, T., DeLorenzo, D.M., Gao, Y., Berla, B., Kim, S.J., Foston, M., Moon, T.S., Dantas, G., 2018a. Multi-omic elucidation of aromatic catabolism in adaptively evolved *Rhodococcus opacus*. *Metab. Eng.* 49, 69–83.
- Henson, W.R., Hsu, F.-F., Dantas, G., Moon, T.S., Foston, M., 2018b. Lipid metabolism of phenol-tolerant *Rhodococcus opacus* strains for lignin bioconversion. *Biotechnol. Biofuels* 11, 339.
- Holder, J.W., Ulrich, J.C., DeBono, A.C., Godfrey, P.A., Desjardins, C.A., Zucker, J., Zeng, Q., Leach, A.L.B., Ghiviriga, I., Dancel, C., Abee, T., Gevers, D., Kodira, C.D., Desany, B., Affourtit, J.P., Birren, B.W., Sinskey, A.J., 2011. Comparative and functional genomics of *Rhodococcus opacus* PD630 for biofuels development. *PLoS Genet.* 7, e1002219.
- Hollinshead, W.D., Henson, W.R., Abernathy, M., Moon, T.S., Tang, Y.J., 2015. Rapid metabolic analysis of *Rhodococcus opacus* PD630 via parallel ¹³C-metabolite fingerprinting. *Biotechnol. Bioeng.* 113, 91–100.
- Hollinshead, W.D., Rodriguez, S., Martin, H.G., Wang, G., Baidoo, E.E.K., Sale, K.L., Keasling, J.D., Mukhopadhyay, A., Tang, Y.J., 2016. Examining *Escherichia coli* glycolytic pathways, catabolite repression, and metabolite channeling using *Apfk* mutants. *Biotechnol. Biofuels* 9, 212.
- Janusz, G., Pawlik, A., Sulej, J., Swiderska-Burek, U., Jarosz-Wilkolazka, A., Paszczynski, A., 2017. Lignin degradation: microorganisms, enzymes involved, genomes analysis and evolution. *FEMS (Fed. Eur. Microbiol. Soc.) Microbiol. Rev.* 41, 941–962.
- Jiang, W., Jiang, Y., Bentley, G.J., Liu, D., Xiao, Y., Zhang, F., 2015. Enhanced production of branched-chain fatty acids by replacing β -ketoacyl-(acyl-carrier-protein) synthase III (*FabH*). *Biotechnol. Bioeng.* 112, 1613–1622.
- Kaneda, T., 1966. Biosynthesis of branched-chain fatty acids: IV. Factors affecting relative abundance of fatty acids produced by *Bacillus subtilis*. *Can. J. Microbiol.* 12, 501–514.
- Kukor, J.J., Olsen, R.H., 1991. Genetic organization and regulation of a meta-cleavage pathway for catechols produced from catabolism of toluene, benzene, phenol, and cresols by *Pseudomonas pickettii* PKO1. *J. Bacteriol.* 173, 4587–4594.
- Kurosawa, K., Laser, J., Sinskey, A., 2015. Tolerance and adaptive evolution of triacylglycerol-producing *Rhodococcus opacus* to lignocellulose-derived inhibitors. *Biotechnol. Biofuels* 8, 76.
- Langmead, B., Salzberg, S.L., 2012. Fast gapped-read alignment with Bowtie 2. *Nat. Methods* 9, 357–359.
- Le, R.K., Das, P., Mahan, K.M., Anderson, S.A., Wells Jr., T., Yuan, J.S., Ragauskas, A.J., 2017. Utilization of simultaneous saccharification and fermentation residues as feedstock for lipid accumulation in *Rhodococcus opacus*. *Amb. Express* 7, 185.
- Li, H., Handsaker, B., Wysoker, A., Fennell, T., Ruan, J., Homer, N., Marth, G., Abecasis, G., Durbin, R., 2009. The sequence alignment/map format and SAMtools. *Bioinformatics* 25, 2078–2079.
- Liao, Y., Smyth, G.K., Shi, W., 2014. featureCounts: an efficient general purpose program for assigning sequence reads to genomic features. *Bioinformatics* 30, 923–930.
- Linger, J.G., Vardon, D.R., Guarnieri, M.T., Karp, E.M., Hunsinger, G.B., Franden, M.A., Johnson, C.W., Chupka, G., Strathmann, T.J., Pienkos, P.T., Beckham, G.T., 2014. Lignin valorization through integrated biological funneling and chemical catalysis. *Proc. Natl. Acad. Sci. Unit. States Am.* 111, 12013–12018.
- Long, C.P., Gonzalez, J.E., Feist, A.M., Palsson, B.O., Antoniewicz, M.R., 2017. Fast growth phenotype of *E. coli* K-12 from adaptive laboratory evolution does not require intracellular flux rewiring. *Metab. Eng.* 44, 100–107.
- Love, M.I., Huber, W., Anders, S., 2014. Moderated estimation of fold change and dispersion for RNA-seq data with DESeq2. *Genome Biol.* 15, 550.
- Madsen, R.B., Jensen, M.M., Mørup, A.J., Houlberg, K., Christensen, P.S., Klemmer, M., Becker, J., Iversen, B.B., Glasius, M., 2016. Using design of experiments to optimize derivatization with methyl chloroformate for quantitative analysis of the aqueous phase from hydrothermal liquefaction of biomass. *Anal. Bioanal. Chem.* 408, 2171–2183.
- Neidhardt, F.C., Ingraham, J.L., M Schaechter, M., 1990. *Physiology of the Bacterial Cell. A Molecular Approach*. Sinauer Associates Inc, Sunderland, MA.
- Pond, J.L., Langworthy, T.A., 1987. Effect of growth temperature on the long-chain diols and fatty acids of *Thermomicrobium roseum*. *J. Bacteriol.* 169, 1328–1330.
- Ragauskas, A.J., Beckham, G.T., Bidy, M.J., Chandra, R., Chen, F., Davis, M.F., Davison, B.H., Dixon, R.A., Gilna, P., Keller, M., Langan, P., Naskar, A.K., Saddler, J.N., Tschaplinski, T.J., Tuskan, G.A., Wyman, C.E., 2014. Lignin valorization: improving lignin processing in the biorefinery. *Science* 344, 1246843 6185.
- Ragauskas, A.J., Williams, C.K., Davison, B.H., Britovsek, G., Cairney, J., Eckert, C.A., Frederick, W.J., Hallett, J.P., Leak, D.J., Liotta, C.L., Mielenz, J.R., Murphy, R., Templer, R., Tschaplinski, T., 2006. The path forward for biofuels and biomaterials. *Science* 311, 484–489.
- Saa, L., Jaureguibeitia, A., Largo, E., Llama, M.J., Serra, J.L., 2010. Cloning, purification and characterization of two components of phenol hydroxylase from *Rhodococcus erythropolis* UPV-1. *Appl. Microbiol. Biotechnol.* 86, 201–211.
- Schuetz, R., Kuepfer, L., Sauer, U., 2007. Systematic evaluation of objective functions for predicting intracellular fluxes in *Escherichia coli*. *Mol. Syst. Biol.* 3, 119.
- Sridevi, V., V V Chandana Lakshmi, M., Manasa, M., Sravani, M., 2012. Metabolic pathways for the biodegradation of phenol. *Int. J. Eng. Sci. Adv. Technol.* 2, 695–705.
- Studer, M.H., DeMartini, J.D., Davis, M.F., Sykes, R.W., Davison, B., Keller, M., Tuskan, G.A., Wyman, C.E., 2011. Lignin content in natural *Populus* variants affects sugar release. *Proc. Natl. Acad. Sci. Unit. States Am.* 108, 6300–6305.
- Szökö, J., Rucká, L., Šimčíková, M., Halada, P., Nešvera, J., Pátek, M., 2014. Induction and carbon catabolite repression of phenol degradation genes in *Rhodococcus erythropolis* and *Rhodococcus jostii*. *Appl. Microbiol. Biotechnol.* 98, 8267–8279.
- Valdivia, M., Galan, J.L., Laffarga, J., Ramos, J.-L., 2016. Biofuels 2020: biorefineries based on lignocellulosic materials. *Microb. Biotechnol.* 9, 585–594.
- Wheeldon, I., Christopher, P., Blanch, H., 2017. Integration of heterogeneous and biochemical catalysis for production of fuels and chemicals from biomass. *Curr. Opin. Biotechnol.* 45, 127–135.
- Xie, S., Sun, S., Lin, F., Li, M., Pu, Y., Cheng, Y., Xu, B., Liu, Z., da Costa Sousa, L., Dale, B.E., Ragauskas, A.J., Dai, S.Y., Yuan, J.S., 2019. Mechanism-guided design of highly

- efficient protein secretion and lipid conversion for biomanufacturing and biorefining. *Adv. Sci.* 1801980.
- Yaguchi, A., Robinson, A., Mihealsick, E., Blenner, M., 2017. Metabolism of aromatics by *Trichosporon oleaginosus* while remaining oleaginous. *Microb. Cell Factories* 16, 206.
- Yi, X., Dean, A.M., 2016. Phenotypic plasticity as an adaptation to a functional trade-off. *eLife* 5, e19307.
- Yoneda, A., Henson, W.R., Goldner, N.K., Park, K.J., Forsberg, K.J., Kim, S.J., Pesesky, M.W., Foston, M., Dantas, G., Moon, T.S., 2016. Comparative transcriptomics elucidates adaptive phenol tolerance and utilization in lipid-accumulating *Rhodococcus opacus* PD630. *Nucleic Acids Res.* 44, 2240–2254.
- You, L., Page, L., Feng, X., Berla, B., Pakrasi, H.B., Tang, Y.J., 2012. Metabolic pathway confirmation and discovery through (13)C-labeling of proteinogenic amino acids. *J. Vis. Exp. : JoVE.* 3583.
- Young, J.D., 2014. INCA: a computational platform for isotopically non-stationary metabolic flux analysis. *Bioinformatics* 30, 1333–1335.